Evaluation of RMS Current in AC Power Wires Using a High-Speed Infrared System

Błażej Torzyk, Bogusław Więcek
Lodz University of Technology, Institute of Electronics, Al. Politechniki 10, B-9 building, 93-590 Lodz, Poland

Abstract: This paper presents a new method of the effective value (RMS) of alternating current (AC) in power wires based on infrared radiation (IR) measurement using a high-speed medium-wavelength infrared (MWIR) camera. The method called "2-ω" involves measurement of the 100 Hz harmonic of temperature (T_{100}) and is supported by signal analysis in the frequency domain. The article discusses the issue of non-sinusoidal alternating current, which causes much more difficult analyzes compared to sinusoidal current with a frequency of 50/60 Hz. The simulation and measurement results for different current shapes obtained in typical power systems like: a phase-controlled switching regulator, half-wave and full-wave rectifiers, and finally the nonlinear distortion of the AC current due to saturation of the magnetic core, are presented and confirm the linear relation of $T_{100} \sim I^2_{RMS}$. The main advantage of proposed method is the independence of the measurement results from environmental conditions.

Keywords: power wires; frequency analysis, non-sinusoidal AC current, infrared camera, radiation temperature measurement, current measurement

1. Introduction

The root mean square current (RMS) is one of the main parameters describing the electric current in electricity distribution systems. There are different methods and equipment for measuring the effective current value in a contact and non-contact manner [1–3, 29–32]. Due to the conversion of electrical energy using power converters, depending on the type of load, sinusoidal current no longer occurs [4, 5]. This significantly affects the accuracy of the measurement. Nowadays, the diverse nature of the operation of electrical equipment and the variety of electrical receivers is one of the main reasons for the need to constantly monitor the parameters and quality of generated, transmitted and processed electricity [1, 4]. Currently, there are a few standard methods for the measurement of RMS current in DC and AC power networks.

1.1. Hall-effect current sensor

Sensors using the Hall-effect are most often used, among others, to monitor the effective value of current in electric drives, automotive applications and power conversion systems [2, 3, 6]. In the Hall-effect sensor (fig. 1), under the influence of a perpendicularly incident magnetic flux, the distribution of carriers changes, which generates an output Hall voltage. Technological development of semiconductors, mainly in the field of materials engineering (e.g. InSb, GaAs, InAs compounds), leads to miniaturization and cost reduction and allows for increased precision and extension of the measurement range of Hall-sensors [1, 7]. Hall-effect sensors are not the passive devices and they require a small DC external power source [8].

The output voltage of the sensor corresponds to the value of the measured current and is usually at the level of μV. Therefore, the signal requires amplification and further processing in order to reduce the measurement errors [9, 10]. Hall-effect sensor allows measuring the DC and AC current with the frequency up to $f_{max} = 250$ kHz [6]. Performing measurements in the AC domain causes difficulties resulting from fluctuations of the alternating magnetic field as a consequence of the core demagnetization. In more advanced applications, in order to

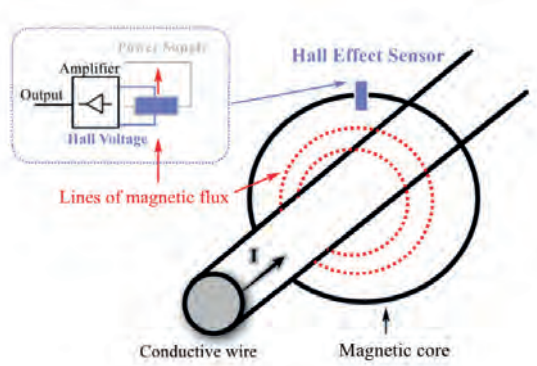

Fig. 1. The configuration of current measurement method using the Hall-effect sensor
Rys. 1. Konfiguracja metody pomiaru prądu z wykorzystaniem czujnika Halla

Autor korespondujący:
Błażej Torzyk, blazej.torzyk@p.lodz.pl

Artykuł recenzowany
nadesłany 22.04.2024 r., przyjęty do druku 01.07.2024 r.

eliminate the measurement errors, two Hall-effect sensors can be implemented, one for static and second for dynamic measurement in the oscillating magnetic field [6].

1.2. Inductive sensor

Current transformers are typical passive elements developed to measure high current values, especially for monitoring and maintaining the supply of electricity to power systems. The operation of current transformers consists in inducing the oscillating magnetic field in a core by a current in a wire – the primary winding. In the older solutions, the power is directed to the secondary winding with a large number of turns in order to measure the voltage proportional to the current in the wire. Nowadays, current transformer subjects the signal from the secondary winding to further electronic processing as shown in fig. 2 [11].

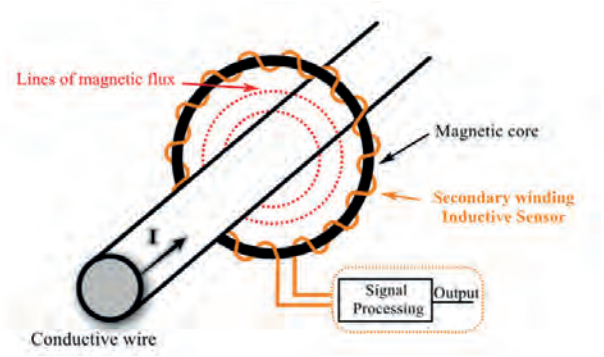

Fig. 2. The configuration of current measurement method using an inductive sensor (current transformer)
Rys. 2. Konfiguracja sposobu pomiaru prądu z wykorzystaniem czujnika indukcyjnego (przekładnika prądowego)

Current transformers enable the recording of alternating current over a wide range and a sufficient range of frequency values with high accuracy. Attempting to connect direct current may saturate the ferromagnetic core, which may lead to permanent damage to the transformer. A hybrid system operating in parallel with the Hall-effect (fig. 1) and an inductive sensor (fig. 2) can be used to measure both direct and alternating currents simultaneously [11, 12].

When performing periodic or operational measurements of a power system with an inductive sensor, the stiff ferromagnetic core causes difficulties. Weight, dimensions and lack of flexibility significantly hinder the use of inductive sensors. This problem can be solved by implementing the Rogowski coil (converter) – fig. 3. The main difference from a typical current transformer is the lack of a ferromagnetic core. An additional electronics amplifies the obtained voltage signal. The non-magnetic core ensures flexibility and no changes in cross-section along the entire length of the secondary winding. This solution reduces the errors of current measurement resulting from changes in the magnetic field and the position of the tested conductor and ensures a linear character of changes of the output signal vs. the monitored current [8, 13].

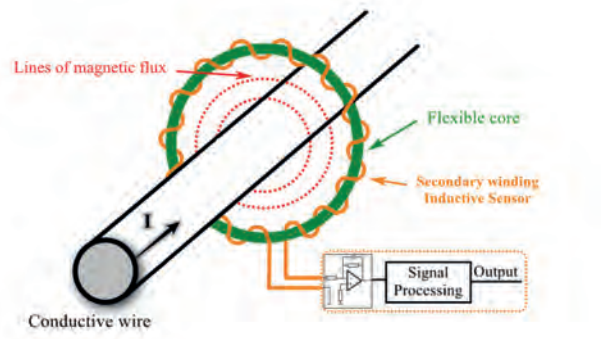

Fig. 3. The Rogowski coil (converter) – working principle
Rys. 3. Cewka Rogowskiego (przetwornik) – zasada działania

Measurement capabilities of the Rogowski coils of AC can reach a range of 0.08 A – 30 kA and the frequency bandwidth of 0.1 Hz – 1 GHz [14, 33]. Additional advantages, such as low production costs and full electrical insulation from the tested conductor, make the Rogowski coil one of the most commonly used instrument for measuring alternating current today [13, 14].

1.3. Shunt resistor

A shunt resistor is an alternative solution for current measurement, mainly in terms of cost and simple implementation as presented in fig. 4. The measurement principle is based on the voltage drop on a resistor characterized by a very low resistance value – usually at the level of μΩ – mΩ [15, 17]. The obtained voltage is amplified and subjected to subsequent post-processing [15, 16]. Shunt resistors enable measurement of current values in the mA – kA range and frequencies of 10 Hz – 100 kHz [15]. Significant value of current, as well as the continuous nature of the recording with a variable load, force the shunt resistors to maintain the appropriate temperature drift, independently of time and frequency. The value of the temperature coefficient of the resistance should not exceed 0.05 – 0.62 $\mu\Omega/(\Omega \cdot K)$ in the full measuring range [3, 18].

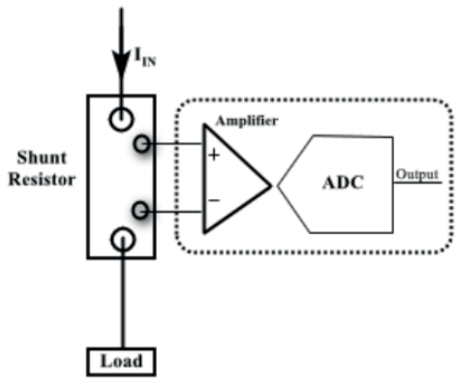

Fig. 4. Shunt resistor – basics of construction
Rys. 4. Rezystor bocznikowy – podstawy budowy

The second type of shunts, so-called coaxial shunts are used in power applications to ensure proper measurement parameters at high frequency range. Such applications are only possible when using specially developed shunts with reduced parasitic inductance. The operation of this type of shunts does not change, while the size, number of elements and the level of complexity of the construction of the entire system increase proportionally to the range of measured electric current value [3, 16]. Shunts of this type can offer the GHz bandwidth, which is demanded in modern industrial and telecommunications solutions [19].

1.4. Non-sinusoidal RMS currents measurement systems

The presented methods of measuring alternating and direct currents must show significant endurance to changes in the power level and electrical nature of the load [5]. The implementation of newer solutions in power conversion systems based on modern power semiconductor devices introduce non-linear distortions, which in turn generate harmonics of the measured signal [4]. The influence of harmonics is reflected in the deterioration of the power factor (PF) [5]. Therefore, various methods of measuring the current value are used [11, 20] in order to monitor and analyze the quality of electrical energy [21, 34].

The time-varying waveform of the AC power signal requires measurement of the $I_{RMS(tot)}$ current, taking into account all signal components (harmonics). Measuring systems of this type, that

are used in electricity distribution systems for continuous monitoring of energy quality, are known as the Advanced Metering Infrastructure system (AMI) [22]. More and more professional and portable digital multimeters offer True-RMS, PF and THD (Total harmonic Distortion) measurements [11]. The available measurement methods focus on indirect or direct measurement of the instantaneous value of alternating current and subsequent data processing. Professional measuring equipment for the frequency f = 50 Hz of the electrical network records a sequence of 10 signal periods (in the time window t = 200 ms) in order to determine the I_{RMS} value. Further additional averaging is then performed to meet the appropriate standards [31, 32, 34].

The article presents a measurement methodology for estimating the I_{RMS} value of sinusoidal and non-sinusoidal alternating current using a fast infrared (IR) system. The presented experiments concern the validation of the "2-ω" method [23, 24, 25, 27, 28] for various alternating currents, such as: sinusoidal and phase-controlled currents for a switching angle of $\varphi = 90°$ (e.g. implemented in a triac controller), as well as for currents in half and full-wave rectifiers. The obtained results confirm the effectiveness of the proposed method for measuring non-sinusoidal alternating current. The proposed method increases application possibilities and creates an opportunity for the development of cheap, portable IR systems for non-contact I_{RMS} measurement in power systems.

2. Theory and methods

The current in the wire generates both power loss and temperature rise. Due to temporal changes of alternating current, the temperature also changes. If the current is not sinusoidal, the temperature signal contains harmonics. In the general case, these harmonic components are at double of the fundamental frequency because the power dissipated in the wire varies with the square of the electric current.

The proposed method is based on the non-contact IR measurement using a high-speed IR system to extract high-frequency temperature harmonics. These components have a small amplitude, because each dynamically heated thermal object behaves as an inertial thermal system that rapidly dampens high-frequency temperature signals. It can be shown that the amplitudes of the higher-order components of the temperature spectrum are of the order of 1 mK and below. This means that the special signal processing methods are needed to measure such low temperature value. Note that a typical cooled photon thermal imaging camera can directly record a temperature signal above Noise Equivalent Temperature Difference (NETD), which at best reaches 15 mK. In addition, as mentioned earlier [25], the main advantage of using high-frequency spectral components to evaluate RMS current is that they are insensitive to environmental conditions such as convective and radiation cooling, wind, solar radiation and humidity. Ultimately, from an engineering point of view, reconstruction the current using the harmonics of temperature leads to the solution of the inverse problem. As a result, the RMS current, power loss and total harmonic distortion (THD) can be evaluated as well. The concept of the proposed method is shown in fig. 5.

2.1. Spectrum of electrical power dissipated in a wire

Consider the various shapes of power wires as shown in fig. 6. For theoretical analysis, wires can be defined as one-dimensional electrothermal objects in which the flowing current dissipates the energy causing the temperature rise.

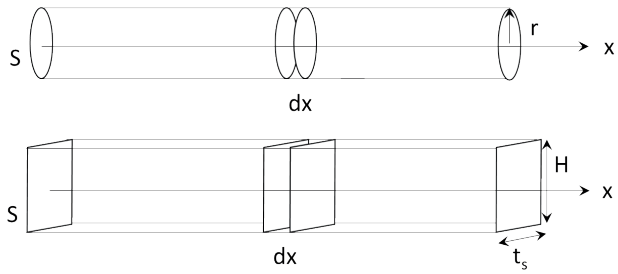

Fig. 6. Geometries of electrical wires
Rys. 6. Geometrie przewodów elektrycznych

In general, the current in the power wire is non-sinusoidal and contains various harmonic components. The power dissipated in the wire is proportional to the square of the current.

$$p(t) \sim \left[\sum_{i=1}^{n} I_i \sin\left(i\omega t + \varphi_i\right)\right]^2 \tag{1}$$

where I_i are the amplitudes of the current harmonic components, for $i = 1, \ldots, n$, and mean value of current is equal to zero.

In order to analyze the temperature harmonics with an IR system, the volumetric power density p_v in the wire needs to be estimated.

$$p_v = \frac{dP}{dV} = \frac{\rho dx}{SdV} I_{rms}^2 = \frac{\rho}{S^2} I_{rms}^2 = \frac{\rho}{2S^2} \sum_{i=1}^{n} I_i^2 \tag{2}$$

where: ρ – material electrical resistivity, S – cross-section area of the wire, I_i – amplitudes of harmonic components of the current.

As is well known nonlinear operations on the signals changes their frequencies and generates sometimes a very distinctive spectral pattern due to the intermodulation effect. Squaring the

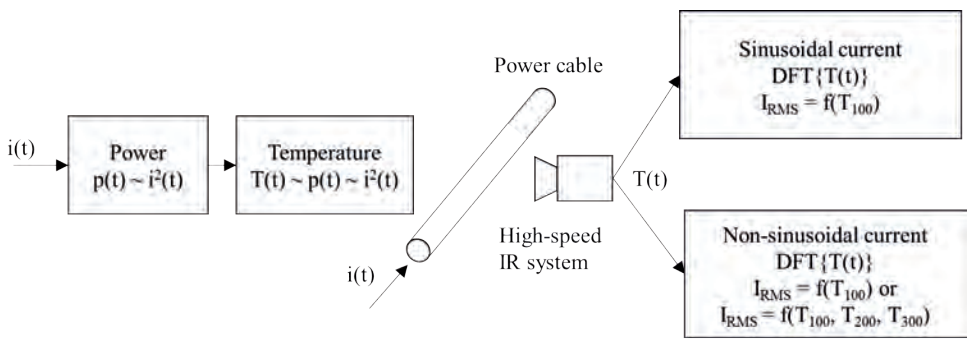

Fig. 5. The concept of the proposed method
Rys. 5. Koncepcja proponowanej metody

current doubles the harmonic frequencies. In the simple case of the 50 Hz sinusoidal current, the power and temperature spectra contain the 100 Hz component only. Using the basic trigonometric rules it is possible to obtain this harmonic components.

$$\left.\begin{aligned} i(t) &= I\sin(\omega t) \\ i^2(t) &= \frac{1}{2}I^2\left[1-\cos(2\omega t)\right] \end{aligned}\right\} \tag{3}$$

For non-sinusoidal currents, the spectrum of the power dissipated in the wire expands significantly. The analysis becomes more difficult due to the intermodulation effect caused by the square of the current. In consequence, the multiplications of harmonic signals with different amplitudes and phases generates the additional differential and summation components of the temperature spectrum. For different current harmonic contents, there are different configurations of the power and temperature spectra, as shown in table 1.

For example, for the very typical case of two odd spectral components, the power spectrum of $i^2(t)$ signal can be represented by second, fourth and sixth components as shown in equation (4):

$$\left.\begin{aligned} i(t) &= I_1\sin(\omega t+\varphi_1)+I_3\sin(3\omega t+\varphi_3) \\ i^2(t) &= \frac{1}{2}I_1^2+\frac{1}{2}I_3^2-\frac{1}{2}I_1^2\cos(2\omega t+2\varphi_1)+I_1I_3\cos(2\omega t+\varphi_3-\varphi_1)- \\ &\quad +I_1I_3\cos(4\omega t+\varphi_3+\varphi_1)-\frac{1}{2}I_3^2\cos(6\omega t+2\varphi_3) \end{aligned}\right\} \tag{4}$$

2.2. Thermal impedance

A power line can be assumed to be a piece of metal with a volume $dV = S{\cdot}dx$ and a dissipated power density p_v. The energy balance equation for both geometries shown in fig. 7 can be expressed as:

$$\left.\begin{aligned} p_{v1}(t) &= c_v\frac{dT_1(t)}{dt}+\frac{2h}{r}T_1(t) \\ p_{v2}(t) &= c_v\frac{dT_2(t)}{dt}+2h\left(\frac{1}{t_s}+\frac{1}{H}\right)T_2(t) \end{aligned}\right\} \tag{5}$$

where h is the convective heat transfer coefficient, c_v is the volumetric thermal capacity, r is the radius of the cylindrical wire, t_s is the thickness and H is the height of the flat wire.

Since the thermal system is linear for a small range of temperature changes at high frequency, for a sinusoidal power excitation with the angular frequency ω, the temperature is also sinusoidal.

$$\left.\begin{aligned} T_1(j\omega t) &= \frac{p_v}{j\omega c_v+\frac{2h}{r}} = \frac{p_{vm}}{j\omega c_v+\frac{2h}{r}}e^{j\omega t} \\ T_2(j\omega t) &= \frac{p_{vm}}{j\omega c_v+2h\left(\frac{1}{t_s}+\frac{1}{H}\right)}e^{j\omega t} \end{aligned}\right\} \tag{6}$$

For typical thermal parameters of a power wire made of steel or copper and similar cooling condition, for $\omega > 2{\cdot}\pi{\cdot}50$ 1/s, the following relations are valid:

$$\left.\begin{aligned} \omega c_v &\gg \frac{2h}{r} \\ \omega c_v &\gg 2h\left(\frac{1}{t_s}+\frac{1}{H}\right) \end{aligned}\right\} \tag{7}$$

In result, regardless of the power wire geometry, the temperature oscillates with the same angular frequency ω and phase delay approximately equal to $-\pi/2$.

$$T(j\omega t) \approx \frac{p_{vm}}{j\omega c_v}e^{j\omega t} = \frac{p_{vm}}{\omega c_v}e^{j\left(\omega t-\frac{\pi}{2}\right)} \tag{8}$$

Finally, the thermal impedance takes a form:

$$Z_{th}(j\omega) \approx \frac{1}{j\omega c_v dV} \tag{9}$$

Table 1. Harmonic orders of current vs. power and temperature
Tabela 1. Rzędy harmonicznych prądu w funkcji mocy i temperatury

Harmonic order				
Current	1	1, 3	1, 3, 5	1, 2, 3, 4
Power and temperature	2	2, 4, 6	2, 4, 6, 8, 10	1, 2, 3, 4, 5, 6, 7, 8

Table 2. Thermal impedance values for chosen frequencies for different wires
Tabela 2. Wartości impedancji cieplnej dla wybranych częstotliwości dla różnych przewodów

Frequency Hz	Copper		Steel	
	$\mathrm{Re}\{Z_{th}\}\times10^{14}$ K/W	$\mathrm{Im}\{Z_{th}\}\times10^{9}$ K/W	$\mathrm{Re}\{Z_{th}\}\times10^{13}$ K/W	$\mathrm{Im}\{Z_{th}\}\times10^{9}$ K/W
50	0.3622	–0.9362	0.2623	–0.8872
100	0.0905	–0.4681	0.0656	–0.4436
150	0.0402	–0.3121	0.0291	–0.2957
200	0.0226	–0.2341	0.0164	–0.2218
250	0.0145	–0.1872	0.0105	–0.1774
300	0.01	–0.1560	0.0073	–0.1479

The simple thermal model presented above can lead to important conclusions. First, the thermal impedance for frequencies $f > 50$ Hz is purely capacitive and consequently varies inversely with frequency as in equation (9).

Assume the analysis for a cylindrical and flat wires made of cooper and steel with the following parameters: $c_v = 3.5 \cdot 10^6$ J/m³K, $h = 10$ W/m²K, $H = 0.03$ m, $r = 0.0006$ m, $t_s = 0.005$ m and $dV = 1$ m³. Simulated exemplary results for Z_{th} are summarized in table 2.

Analyzing the values of thermal impedance in table 2 obtained using physical and geometrical parameters of the wire, it possible to notice that e.g. for the cooper wire, for f = 100 Hz, $\mathrm{Re}\{Z_{th}\} = 0.0905 \cdot 10^{-14}$ K/W and $\mathrm{Im}\{Z_{th}\} = -0.4681 \cdot 10^{-9}$ K/W. In consequence, $\mathrm{tg}(\mathrm{Im}/\mathrm{Re}) \approx -0.5 \cdot 10^6$ and corresponding $\arg\{Z_{th}\} = -89.999°$.

Simple modelling of the thermal impedance of the wire $Z_{th}(j\omega)$ leads to practical conclusions helpful in the measurement of temperature, power and current. The ratio of the 100 and 200 Hz amplitudes for temperature is two times greater than the same ratio for the power and $i^2(t)$ signals. In addition, due to the highly capacitive nature of the thermal system, for $f \geq 50$ Hz, there is a $-\pi/2$ phase delay between temperature and power for high-frequency spectral components. All these conclusions simplify the reconstruction of the RMS value of the current from the high-frequency range of temperature spectrum.

2.3. Temperature spectrum and current harmonics reconstruction

As mentioned above, due to the highly capacitive thermal structure of the power wire for the frequency $f \geq 50$ Hz, the phase shift between temperature and power is very close to $-\pi/2$. In addition, increasing the frequency proportionally reduces the imaginary part and modulus of thermal impedance.

As an example, consider the current consisting of the fundamental and 3rd harmonics only. According to the table 1 and equation (4), the amplitudes of the harmonic components of temperature can be represented as:

$$T_i = \left|Z_{thi}\right| e^{-j\frac{\pi}{2}} \rho \frac{dx}{S} f_i\left(I_1, I_3, \varphi_1, \varphi_3\right) \tag{10}$$

for i = 2, 4, 6, i.e. for $f = \{100, 200, 300\}$ Hz, where functions f_i take the forms:

$$\left.\begin{aligned} \mathrm{Re}\left\{f_2\right\} &= -\frac{1}{2} I_1^2 \cos\left(2\varphi_1\right) + I_1 I_3 \cos\left(\varphi_3 - \varphi_1\right) \\ \mathrm{Im}\left\{f_2\right\} &= -\frac{1}{2} I_1^2 \sin\left(2\varphi_1\right) + I_1 I_3 \sin\left(\varphi_3 - \varphi_1\right) \end{aligned}\right\} \tag{11}$$

$$\left.\begin{aligned} \mathrm{Re}\left\{f_4\right\} &= -I_1 I_3 \cos\left(\varphi_3 + \varphi_1\right) \\ \mathrm{Im}\left\{f_4\right\} &= -I_1 I_3 \sin\left(\varphi_3 + \varphi_1\right) \end{aligned}\right\} \tag{12}$$

$$\left.\begin{aligned} \mathrm{Re}\left\{f_6\right\} &= -\frac{1}{2} I_3^2 \cos\left(2\varphi_3\right) \\ \mathrm{Im}\left\{f_6\right\} &= -\frac{1}{2} I_3^2 \sin\left(2\varphi_3\right) \end{aligned}\right\} \tag{13}$$

Using (9) and (10), the non-linear system of implicit equations (11)–(13) can be solved with respect to the unknowns I_1, I_3, φ_1, φ_3.

$$f_i\left(I_1, I_3, \varphi_1, \varphi_3\right) = \frac{\omega_i c_v S^2}{\rho} T_i e^{j\frac{\pi}{2}} \tag{14}$$

Although the system of equations (11)–(13) is overdetermined (6 equations with 4 unknowns), it is better to choose the first 2 of them (11) and (12), because the values of temperature harmonics amplitudes T_i decrease rapidly with frequency. Moreover, the functions f_i are implicit with respect to harmonic amplitudes and phases. As a result, an optimization must be applied to obtain a solution to the posed inverse problem. Finally, the RMS value of the current can be calculated classically as:

$$I_{RMS} = \sqrt{\frac{I_1^2 + I_3^2}{2}} \tag{15}$$

The proposed method also allows to determine the THD factor for the current. It should be emphasized that the coefficient $\frac{\omega_i c_v S^2}{\rho}$ can be treated as a calibration parameter. In practice, the calibration should be carried out experimentally for each power wire independently.

2.4. Approximated evaluation of the RMS value of non-sinusoidal current

As mentioned above, the RMS current evaluation method is suitable for sinusoidal current. Again, it should be noted that the temperature harmonics for $f > 50$ Hz are below the noise level of any IR system and decrease rapidly with frequency. For non-sinusoidal current, the need to take into account higher temperature harmonics causes errors. Moreover, in the general case, the current, power and temperature spectra are infinite and obviously cannot be measured by any IR system.

For this reason, an approximate solution is proposed. It requires calibration for each RMS current measurement configuration. The approach is based on the observation that the RMS value of non-sinusoidal current varies with the square root of the temperature harmonics and in many practical cases, this relationship is linear. The idea is to use the lower-order spectral component of temperature to evaluate the RMS current. It is recommended to use the 100 Hz temperature harmonic component T_{100}. One should not use the 50 Hz component (if exists) due to the effect of power line electromagnetic fields on high-impedance electronics of IR system and the ubiquitous 50 Hz noise in mains-powered systems.

Consider 3 parameters, only one of which changes in each simulation test: the current scaling factor γ, the phase φ_0 of the selected harmonic component varying in the range $(0, \pi)$, and the ratio of the amplitudes of the selected components, e.g. I_1 and I_3.

$$i\left(t\right) = \gamma f\left(t - T_0\right) \tag{16}$$

where $T_0 = \varphi_0/\omega$ and $f(t)$ is the series of harmonic components of the temperature spectrum with different and varying amplitudes.

In order to confirm the linear dependence between RMS current and 100 Hz harmonic of $i^2(t)$ signal which directly corresponds to $T(t)$, the simulations were performed for six different non-sinusoidal currents $i(t)$.

The calculations were carried out for the current consisting of the first two odd harmonics $i(t) = \sin(2\pi ft) + 0.2\sin(3 \cdot 2\pi ft + \varphi_0)$, the current generated by the half-wave and full-wave rectifiers,

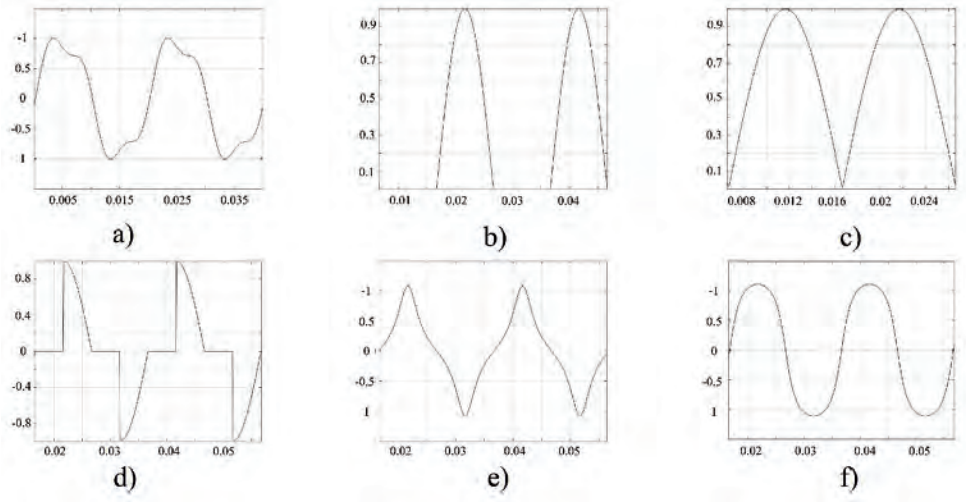

Fig. 7. Different non-sinusoidal currents: (a) $i(t) = \sin(2\pi ft) + 0.2\sin(3\cdot 2\pi ft)$, (b) generated by the half-wave and (c) full-wave rectifiers, (d) obtained from the triac power driver with the switching angle of 90°, (e) supplied by the transformer with magnetic core saturation and (f) from the overdriven circuit

Rys. 7. Różne prądy niesinusoidalne: (a) $i(t) = \sin(2\pi ft) + 0{,}2\sin(3\cdot 2\pi ft)$, (b) generowane przez prostowniki jednopołówkowe i (c) dwupołówkowe, (d) otrzymywane w układzie fazowego sterownia mocą z triakiem dla kąta załączenia 90°, (e) w układzie z transformatorem z nasyceniem rdzenia magnetycznego oraz (f) z obwodu przesterowanego

the current obtained from the triac power driver with the switching angle of $\pi/2$, the current supplied by the transformer with magnetic core saturation and the current from an overdriven circuit – fig. 7.

As shown in fig. 8, the analysis confirmed the linearity of the relationship between the square of RMS current and the square of 100 Hz harmonic. It has to be underlined that there are some special cases when 100 Hz harmonic does not exist in the temperature spectrum or it can be relatively low. Moreover, for square wave AC current, no even single harmonic of temperature occurs. From the power point of view, the square wave current behaves as DC current.

The results of simulations of the relationships of RMS current versus square root of 100 Hz harmonic amplitude of $i^2(t)$ for current consisting of 1st and 3rd harmonics only, with varying amplitude of the 3rd one, are presented in fig. 9. Scaling the current level $i(t)$ by the factor γ changes both the RMS value and 100 Hz harmonic of $i^2(t)$ signal. As expected, this relationship is linear, and also passes through the origin of the coordinate system. In practice, this means that a single measurement is sufficient to calibrate the IR system.

Subsequent calculations were carried out for the current consisting of two first odd harmonics $i(t) = \sin(2\pi ft) + 0.2\sin(3\cdot 2\pi ft + \varphi_0)$, where the phase of the third harmonic varied in the range $\varphi_0 \in (0, \pi)$. The results confirmed the full independence of the 100 Hz component from this phase.

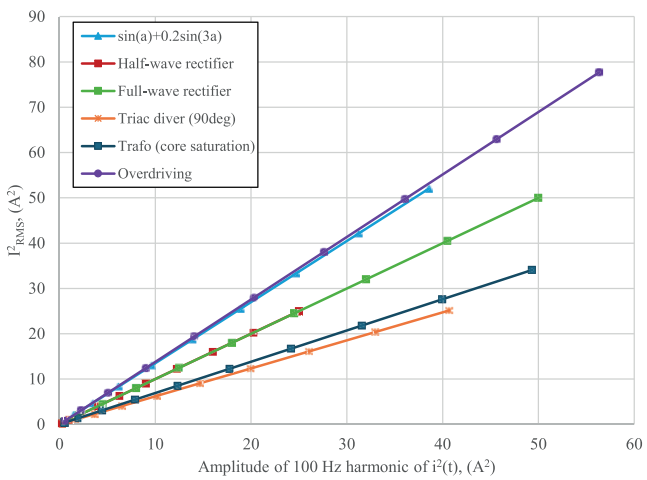

Fig. 8. The square of RMS current value vs. square of 100 Hz harmonic amplitude for $i^2(t)$ for different currents and THD

Rys. 8. Kwadrat wartości skutecznej prądu w funkcji kwadratu amplitudy harmonicznej 100 Hz dla $i^2(t)$, dla różnych prądów i THD

The last and certainly no less important results show the influence of the ratio of the amplitudes of the fundamental and the 3rd harmonic of the considered current. This case seems to be the most important from the point of view of measurement uncertainty with the proposed method. In this case, the amplitude of the 3rd harmonic increases to 20 % of the amplitude of the fundamental harmonic. The result presented in fig. 9 shows that the RMS value of the current deviates from the value for the sinusoidal current by about 2 % only.

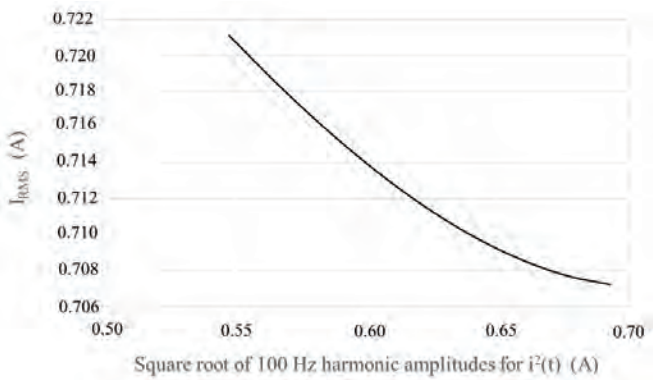

Fig. 9. RMS current value vs. square root of 100 Hz harmonic amplitude for $i^2(t)$, $i(t) = \sin(2\pi ft) + \gamma\sin(3\cdot 2\pi ft)$, f = 50 Hz, $0.02 \le \gamma \le 0.2$

Rys. 9. Wartość skuteczna prądu w funkcji pierwiastka kwadratowego amplitudy harmonicznej 100 Hz dla $i^2(t)$, $i(t) = \sin(2\pi ft) + \gamma\sin(3\cdot 2\pi ft)$, f = 50 Hz, $0.02 \le \gamma \le 0.2$

Uncertainty analysis has already been performed experimentally for a very similar wire in a wind tunnel [25]. The total uncertainty was estimated at ~100 μK. As mentioned earlier, the "2-ω" method requires calibration for each measurement session. Since the uncertainty analysis depends on the IR camera used, it is worth performing it independently for each case.

3. Measurement results

3.1. Experimental setups

Figure 10 presents the block diagram of the experimental set-up. The aim of the experiment was to verify the T_{100} thermal response of the tested steel wire (1) with 1.25 mm cross section diameter, for different types of AC current signals (2): (a) double-sinusoidal, (b) phase-controlled with 90° switching angle (triac driver – BTA41), (c) half-wave rectification (diode

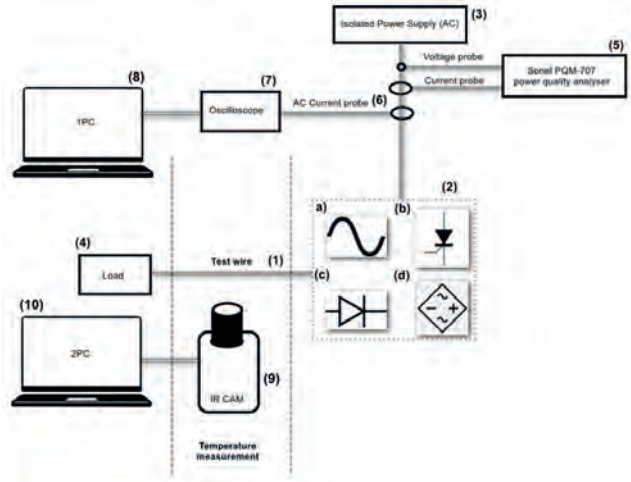

Fig. 10. The block diagram of the experimental set-up
Rys. 10. Schemat blokowy układu doświadczalnego

STTH1512D), (d) full-wave rectification (rectification bridge VS-GBPC2512W). Power was supplied by an isolated power source – NDN AFC-110 (3). The RMS value of alternating current, regardless the type of the AC current signal were in the range of 2.41–6.52 A. The electrical parameters and the quality of electrical power supplied to the load (4), with resistance R = 8 Ω were recorded using the Sonel PQM-707 power quality analyzer (5) and AC current probe AmpFlex A110 (6) coupled with 14 bit acquisition system (7) that was used to record signals on a PC (8) at the sampling frequency f_s = 10 kHz with total number of N = 128 000 samples.

Changes in temperature values were monitored and recorded using a Cedip-Titanium (9), the high-speed Middle Wavelength IR (MWIR) thermal camera with 640 × 512 InSb cooled detector. The IR camera (9) coupled to 2PC (10) recorded temperature changes within 180 seconds, with a frequency of 870 Hz. Data acquisition was carried out using dedicated software on 2PC (10). Figure 12 presents the actual test stand prepared for testing.

Initially the possibility of using an extension ring for steel wire image magnification was taken into account [26], however the preliminary measurement experiments showed that at minimum focusing distance, the camera with its lens offered the better spatial resolution than 100 µm per pixel, thus finally no extension ring was added.

The registration and measurement of image sequences using high-speed IR systems (fig. 11), were carried out 3 times for different current values, and then they were averaged and processed using high-pass and notch digital filter tuned for 100 Hz.

3.2. Signal processing of measured temperature

The harmonics of temperature signal are lower than the noise of the IR system. This means that special signal processing methods must be used to detect and measure the sub-noise signals. Typically, the amplitude of the 100 Hz harmonic is less than 1 mK, while the lowest NETD of today's cameras is equal at most to 15 mK. The proposed and experimentally verified algorithm of RMS current measurement is presented in fig. 13.

First, the DC and low-frequency part of the temperature spectrum is removed by a high-pass (HP) filter. In this study, a Butterworth Infinite Impulse Response (IIR) filter

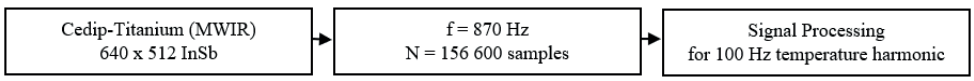

Fig. 11. Processing of image sequences using a high-speed IR systems Cedip-Titanium MWIR cooled camera
Rys. 11. Procedura przetwarzania sekwencji obrazów przy użyciu chłodzonej kamery Cedip-Titanium MWIR

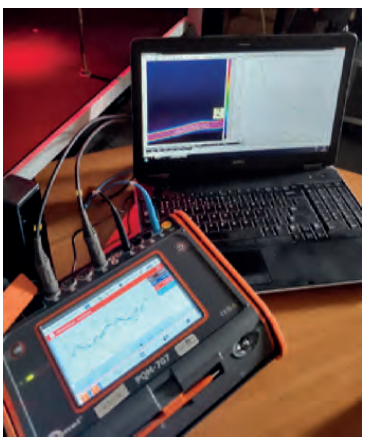

Fig 12. The actual test-bench measuring of RMS current value measurement (AC)
Rys. 12. Rzeczywisty stanowisko pomiaru wartości skutecznej prądu (AC)

with a cut-off frequency f_c = 70 Hz was implemented in the MATLAB environment. Depending on the IR system used, 50 Hz noise with its derivatives may mask the temperature signal emitted by the wires. Additional filtering with cascade notch filters is recommended to reduce the influence of 50 Hz noise. It is good practice to reduce the noise in the signal by measuring the temperature synchronously with the 50 Hz current, but this is not always possible. Incidentally, this solution suffers from an additional signal to be connected, as a result of which the method can no longer be remote and contactless.

In the next step of the proposed method, the Discrete Fourier transform (DFT) is used to obtain the temperature spectrum. Due to the rapid attenuation of temperature signals with increasing frequency and the limited sensitivity of modern IR systems, at most a 6th order harmonic (300 Hz)

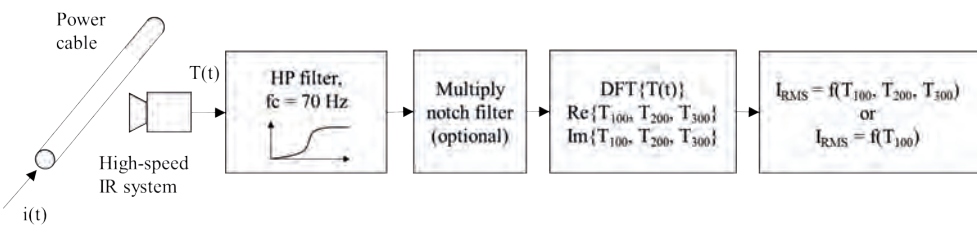

Fig. 13. Proposed signal processing algorithm for I_{RMS} current evaluation from the high-frequency spectrum of temperature
Rys. 13. Algorytm przetwarzania sygnału do wyznaczania wartości I_{RMS} na podstawie widma temperatury

can be detected. This is the main reason why the best solution for RMS current measurement is to use only the 100 Hz temperature harmonic. For the sinusoidal current, this is the only harmonic that exists. For non-sinusoidal current, the monotonic correlation of the 100 Hz harmonic amplitude with the RMS value is helpful. Fortunately, such a correlation occurs for many differently deformed currents.

3.3. Experimental results and discussion

The laboratory experiment begins with a comparison of the temperature frequency spectra in the (100–300) Hz range for a steel wire with a diameter of 1.25 mm for sinusoidal and non-sinusoidal current. The current was supplied by a phase-controlled switching power regulator using a triac. In both measurements, the same current amplitude of about 9 A was settled. The switching-on-phase was either very close to 0° or 90°. For full-time closing of the semiconductor relay, the average wire temperature measured with a thermal imaging camera was 72.15 °C, and for the switching phase 90° it dropped down to 53.04 °C. The measurement lasted 180 seconds.

Figure 14a shows the temporal temperature for a sinusoidal current recorded by the camera after removing the average value. After applying an HP filter with a cutoff frequency of f_c = 70 Hz, the temperature signal looks like noise with a variable amplitude reaching a maximum of about 6 mK – fig. 14b. Stretching this signal to tens of ms reveals oscillations with a period of about 10 ms (f = 100 Hz) – fig. 14c.

The results presented in fig. 15, confirm the correctness of the proposed solution for non-contact measurement of effective current using IR thermography. As expected, the spectrum of a 50 Hz sinusoidal current contains a single harmonic at

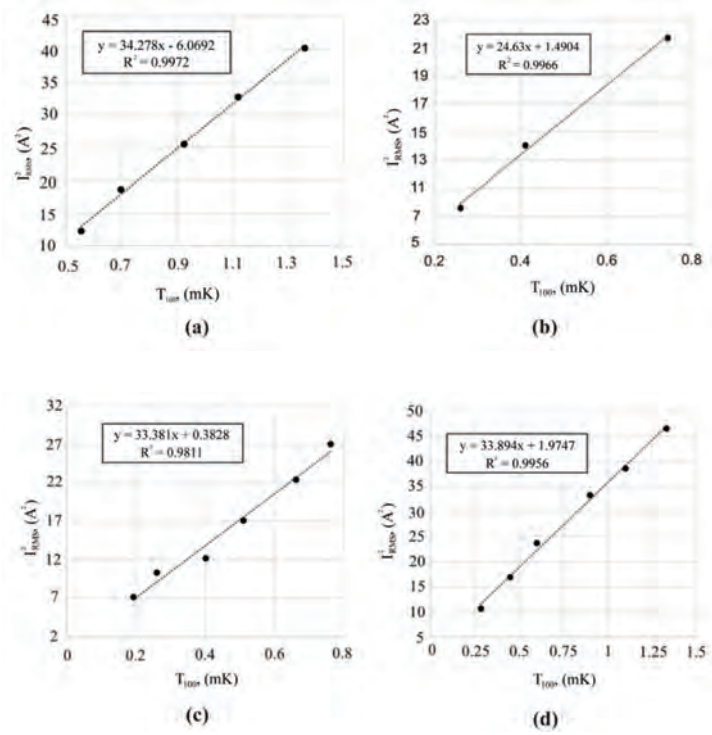

Fig. 16. Relationships $I^2_{RMS} = f(T_{100})$ for different currents: (a) sinusoidal, (b) phase-controlled φ = 90° (triac driver), (c) half-wave rectification, (d) full-wave rectification

Rys. 16. Zależności $I^2_{RMS} = f(T_{100})$ dla różnych przebiegów prądu: (a) sinusoidalny, (b) w układzie sterowania fazowego dla kąta załączania φ = 90° (sterownik z triakiem), (c) prostownika jednopołówkowego, (d) prostownika dwupołówkowy

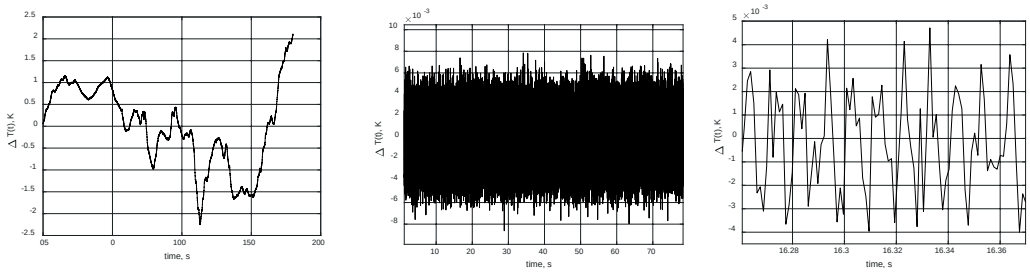

Fig. 14. Temperature signal registered by: (a) the sensitive thermal camera – (b) after mean value removal and (c) after HP filtering (f_c = 70 Hz, 3rd-order Butterworth IIR filter)

Rys. 14. Sygnał temperatury zarejestrowany przez: (a) czułą kamerę termowizyjną – (b) po usunięciu wartości średniej i (c) po filtracji wysokich częstotliwości (f_c = 70 Hz, filtr Butterworth 3-go rzędu – filtr IIR)

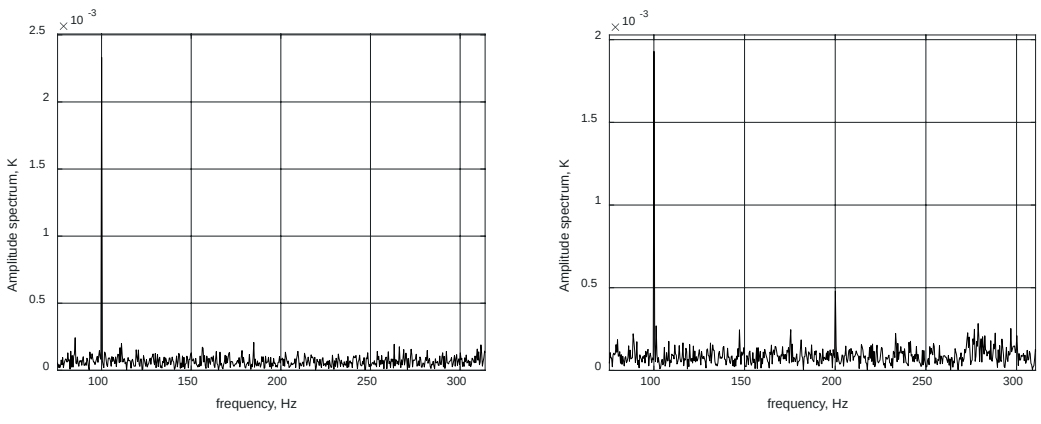

Fig. 15. Spectra of temperature signal for: (a) sinusoidal and (b) π/2 phase switching current

Rys. 15. Widma sygnału temperatury dla prądu: (a) sinusoidalnego i (b) niesinusoidalnego w układzie sterowania fazowego dla kąta załączania π/2

100 Hz. In theory, the temperature spectrum of the $\pi/2$ phase-controlled current has an infinite number of odd-frequency components. As seen in fig. 15, the amplitude of the 200 Hz component is ¼ of the amplitude of 100 Hz harmonic. According to the frequency dependence of the thermal impedance of a wire (table 2), the temperature decreases with frequency. To restore the level of the 200 Hz harmonic of $i^2(t)$, it must be scaled up by a factor of 2. As a result, the 200 Hz harmonic of the $i^2(t)$ signal is half of the 100 Hz harmonic. It fits the theory perfectly.

The final results presented in fig. 16 show the relationship between the RMS value of non-sinusoidal currents and the 100 Hz temperature harmonic for various current shapes and harmonic content. They all show a linear relationship $I^2_{RMS} \sim T_{100}$.

4. Conclusions

The results of the research presented in the article confirmed the effectiveness of the "2-ω" method for measurement of RMS value of AC non-sinusoidal currents. This means that this method is of practical importance for non-contact measurement of effective current using an IR system. This is an indirect approach of electrical parameters' estimation by measuring the 100 Hz temperature harmonic using a sensitive and fast IR technique. The main advantage of using the "2-ω" method is the reliable measurement of the temperature component with a frequency of 100 Hz, regardless of environmental conditions [25]. This is all due to high-frequency temperature measurement and the capacitive nature of the thermal body, which in our case is an energy wire.

On the other hand, a possible disadvantage of the described method is the very weak measured temperature signal, usually of the order of 1 mK, while the noise level of a modern IR photon camera defined by NETD is about 15 mK. This means that advanced signal and image processing must be used to extract the temperature signal from the noise.

We confirmed theoretically and experimentally the linear relationship between the square of the RMS value of the non-sinusoidal current and the amplitude of the 100 Hz temperature harmonic. The value of the measured temperature signal strongly depends on both the frequency and the heat capacity of the measured object. The same technique can be used in countries having the $f = 60$ Hz system for the public electricity grid. This means that calibration is always needed. Thanks to this, after calibration, the measurement is simple, non-contact, fast and reliable – independent from the environmental conditions. The use of an IR camera together with the developed "2-ω" method allows for monitoring and measurement of electrical parameters of a high voltage power line in real time. Investigation can be performed from the ground with an appropriate infrared telescope lens significantly reducing danger during measurement. It is important to emphasize that no imaging system is needed to measure or continuously monitor temperature of an object. It is possible to use cheap, lightweight and inexpensive infrared device with a single detector. Due to the higher sensitivity, it is recommended to use a cooled photon IR system, not the one that is very popular today with a bolometer sensor. Thanks to this, such a system can be easily installed, for example, on an unmanned aircraft. Development of a cheap IR system based on the "2-ω" method for measurement of RMS value of AC currents is the scope of future research.

Acknowledgments

This research was funded by Inkubator Innowacyjności 4.0, grant number, MNISW/2020/326/DIR.

Bibliography

1. Karsenty A., *A Comprehensive Review of Integrated Hall Effects in Macro-, Micro-, Nanoscales, and Quantum Devices*. "Sensors", Vol. 20, No. 15, 2020, DOI: 10.3390/s20154163.
2. Zhang Z., Leggate D., Matsuo T., *Industrial Inverter Current Sensing with three shunt resistors: Limitations and Solutions*. "IEEE Transactions on Power Electronics", 2017, 4577–4586. DOI: 10.1109/TPEL.2016.2596778.
3. Ouameur M., Ziadé F., Le Bihan Y., *Toward a calculable standard shunt for current measurement at 10 A and up to 1 MHz*. "IEEE Transactions on Instrumentation and Measurement", Vol. 68, No. 6, 2019, 2215–2222, DOI: 10.1109/TIM.2018.2884553.
4. El-Goharey H.S.K., Mamdouh W.M., *On-line analysis of power quality problems in non-sinusoidal/non-linear distribution systems*. "Ain Shams Engineering Journal", Vol. 14, No. 9, 2023, DOI: 10.1016/j.asej.2023.102266.
5. Monteiro F.P., Monteiro S.A., Tostes M.E., Bezerra U.H., *Using True RMS Current Measurements to Estimate Harmonic Impacts of Multiple Nonlinear Loads in Electric Distribution Grids*. "Energies", Vol. 12, No. 21, 2019, DOI: 10.3390/en12214132.
6. Crescentini M., Syeda S.F., Gibiino G.P., *Hall-Effect Current Sensors: Principles of Operation and Implementation Techniques*. "IEEE Sensors Journal", Vol. 22, No. 11, 2022, 10137–10151, DOI: 10.1109/JSEN.2021.3119766.
7. Kadri S., *Applications of InAs Hall Effect Sensor*. "Sensors and Transducers Journal", Vol. 119, No. 8, 2010, 22–29.
8. Silventoinen P., Kuisma M., *Review on the Current Measurement systems in Power Electronics*. International Conference on Efficient Welding in Industrial Applications (ICEWIA), Lappeenranta, Finland, 1999.
9. Lalwani A.V., Yalamarthy A.S., Alpert H.S., Holiday M., Eisner S.R., Chapin C.A., Senesky D.G., *Hall-Effect Sensor Technique for No Induced Voltage in AC Magnetic Field Measurements Without Current Spinning*. "IEEE Sensors Journal", Vol. 22, No. 2, 2022, 1245–1251, DOI:10.1109/JSEN.2021.3130527.
10. Liu J., Sanli A.S., Wang Y., Liu Ch., *Error Compensation of closed Loop Hall Effect Current Sensors*. IEEE International Workshop on Applied Measurements for Power Systems (AMPS), Germany, Aachen, September 26–28, 2012.
11. Flores-Arias J.-M., Ortiz-Lopez M., Latorre F.J.Q., Bellido-Outeiriño F.J., Moreno-Muñoz A., *A Memory-Efficient True-RMS Estimator in a Limited-Resources Hardware*. "Energies", Vol. 12, No. 9, 2019, DOI: 10.3390/en12091699.
12. Wang K., Yang X., Li H., Wang L., *A High-Bandwidth Integrated Current Measurement for Detecting Switching Current of Fast GaN Devices*. "IEEE Transactions on Power Electronics", Vol. 33, No. 7, 2018, 6199–6210, DOI: 10.1109/TPEL.2017.2749249.
13. Nanyan A.N., Isa M., Hamid H.A., Rohani M.N.K.H., Ismail B., *The Rogowski Coil Sensor in High Current Application: A Review*. IOP Conference Series Materials Science and Engineering. 2018, Vol. 318, DOI: 10.1088/1757-899X/318/1/012054.
14. Samini M.H., Mahari A., Farahnakin M.A., Mohseni H., *The Rogowski Coil Principles and Applications: A Review*. "IEEE Sensors Journal", Vol. 15, No. 2, 2014, 651–658, DOI: 10.1109/JSEN.2014.2362940.
15. Kato H., Saito M., Takahashi Y., Yoshino K., Domae A., Kiryu S., Nobu-Hisa K., *Development and Evaluation of a Simple Shunt Module for High DC Current Measurement*. "IEEE Transactions on Power Delivery", Vol. 38, No. 3, 2023, 1656–1664, DOI: 10.1109/TPWRD.2022.3224072.

16. Voljc B., Lindic M., Lapuh R., *Direct Measurement of AC Current by Measuring the Voltage Drop on the Coaxial Current Shunt*. "IEEE Transactions on Instrumentation and Measurement", Vol. 58, No. 4, 2009, 863–867, DOI: 10.1109/TIM.2008.2007074.
17. Pogliano U., Bosco G.C., Serazio D., *Coaxial Shunts as AC-DC Transfer Standards of Current*. "IEEE Transactions on Instrumentation and Measurement", Vol. 58, No. 4, 2009, 872–877, DOI: 10.1109/TIM.2008.2008469.
18. Malinowski M., Kubiczek K., Kampik M., *A precision coaxial current shunt for current AC-DC transfer*. "Measurement", Vol. 176, 2021, DOI: 10.1016/j.measurement.2021.109126.
19. Shillaber L., Jiang Y., Ran L., Long T., *Ultrafast Current Shunt* (*UFCS*): *A Gigahertz Bandwidth Ultra Low Inductance Current Sensor*. "IEEE Transactions on Power Electronics", Vol. 37, No. 12, 2022, 15493–15504, DOI: 10.1109/TPEL.2022.3184638.
20. Sydenham P.H., Thorn R., *Handbook of Measuring System Design*, Chapter: 202 Current Measurement, 3 Volume Set, 1st Edition, Wiley, 2005, DOI: 10.1002/0471497398.mm320.
21. Silva J.I., Sousa V., Sarmiento P., Gómez J.R, Viego P.R., Quispe E.C., *Effects of power electronics devices on the Energy quality of an administrative building*. "International Journal of Power Electronics and Drive Systems", Vol. 10, No. 4, 2019, 1951–1960, DOI: 10.11591/ijpeds.v10.i4.pp1951–1960.
22. Mohassel R.R., Fung A., Mohammadi F., Raahemifar K., *A survey on Advanced Metering Infrastructure*. "International Journal of Electrical Power and Energy Systems", Vol. 63, 2014, 473–484. DOI: 10.1016/j.ijepes.2014.06.025.
23. Torzyk B., Więcek B., *A method of RMS current measurement especially in low and medium voltage power lines and cable*. Polish patent submission. No. 428676, 2019.
24. Torzyk B., Więcek B., *Measurement of High-Frequency sub-noise temperature signal and RMS current using a single-detector high-speed IR system*. "Pomiary Automatyka Robotyka", Vol. 27, No. 4, 2023. 53–56, DOI: 10.14313/PAR_250/53.
25. Torzyk B., Więcek B., *Second-Harmonic Contactless Method for Measurement of RMS Current using a standard Infrared Camera*. "IEEE Transactions on Instrumentation and Measurement", Vol. 70, 2021, DOI: 10.1109/TIM.2021.3077676.
26. Kałuża M., Hatzopoulos A., *Application of extension rings in thermography for electronic circuits imaging*. "Quantitative InfraRed Thermography Journal", Vol. 21, 2024, 50–68, DOI: 10.1080/17686733.2022.2146419.

Other sources

27. Torzyk B., Więcek B., *Method of measuring the effective value of current, in particul air in power cables and wires of LV and MV Networks*. Silver Medal for the Invention, 2022 Kaohsiung International Invention & Design EXPO 1–3 December, 2022 Kaohsiung, Taiwan.
28. Torzyk B., Więcek B., *Methode de mesure de la valeur effective du courant*. Silver Medal for the Invention. Geneva inventions, Geneva, 28.04.2023.
29. AEC – Q200: Stress Test Qualification for Passive Components, Automotive Electronics Council Component Technical Committee, 2023
30. IEC 61000-4-7:2002 Electromagnetic compatibility (EMC) – Part 4–7: Testing and measurement techniques – General guide on harmonics and interharmonics measurement and instrumentation, for power supply systems and equipment connected thereto.
31. IEC 61000-4-30:2015 Electromagnetic compatibility (EMC) – Part 4–30: Testing and measurement techniques – Power quality measurement methods.
32. IATF 16949:2016 Quality management system for organizations in the automotive industry, International Automotive Task Force (IATF) standard.
33. Chauvin Arnoux, *A110 AmpFlex flexible sensor*, [https://catalog.chauvin-arnoux.com/fr_en/nf-gb-ampflex--a110-flexible-ac-current-sensors-a110-130.html].
34. IEEE. Standard for Harmonic Control in Electric Power Systems, IEEE Std 519-2022 (Revision of IEEE Std 519-2014), 1–31, 5 Aug. 2022, DOI: 10.1109/IEEESTD.2022.9848440.

Ewaluacja wartości skutecznej RMS prądu przemiennego w przewodach elektroenergetycznych z wykorzystaniem radiacyjnego pomiaru temperatury systemami IR

Streszczenie: Artykuł przedstawia nową metodę pomiaru wartości skutecznej (RMS) prądu przemiennego (AC) w przewodach elektroenergetycznych w oparciu o pomiar promieniowania podczerwonego (IR) za pomocą szybkiej kamery IR, o średniej długości fali (MWIR). Metoda zwana „2-ω", polega na pomiarze harmonicznej temperatury 100 Hz (T_{100}) i analizie sygnału w dziedzinie częstotliwości. W artykule poruszono problematykę niesinusoidalnego prądu przemiennego, który powoduje znacznie trudniejsze analizy w porównaniu z prądem sinusoidalnym o częstotliwości 50/60 Hz. Wyniki symulacji i pomiarów dla różnych kształtów prądu uzyskanych w typowych układach elektroenergetycznych, takich jak: regulator przełączający – sterowany fazowo, prostowniki jednopołówkowe i dwupołówkowe, oraz nieliniowe odkształcenie prądu przemiennego na skutek nasycenia rdzenia magnetycznego, przedstawiono i potwierdzono liniową zależność $T_{100} \sim I^2_{RMS}$. Główną zaletą proponowanej metody jest niezależność wyników pomiarów od warunków środowiskowych.

Słowa kluczowe: przewody zasilające; analiza częstotliwości, niesinusoidalny prąd przemienny, kamera termowizyjna, pomiar radiacyjny temperatury, pomiar prądu

Błażej Torzyk, MSc
blazej.torzyk@p.lodz.pl
ORCID: 0000-0003-4387-2741

He received BSc degree in Electronics and Telecommunication at Technical University of Lodz in 2013 and the MSc degree in Electrical Engineering, specialization Electric Power Engineering in 2015. Currently he is a PhD student at the Electronic Circuits and Thermography Department of Lodz University of Technology. His research interests lie in the fields IR thermography at power electronics systems and devices.

Prof. Bogusław Więcek, PhD DSc
boguslaw.wiecek@p.lodz.pl
ORCID: 0000-0002-5003-1687

Bogusław Więcek is the head of Electronic Circuit and Thermography Division in the Institute of Electronics where he has been working for more than 40 years. His scientific interests are: heat transfer modelling, industrial and biomedical applications of IR thermography and IR system modelling and developments. He is responsible for organizing the largest conference on thermography in Central and Easter Europe every two years "Infrared thermography and thermometry – TTP".